Systems/Circuits

Large Somatic Synapses on Neurons in the Ventral Lateral Lemniscus Work in Pairs

Christina Berger,[1]* Elisabeth M.M. Meyer,[1]* Julian J. Ammer,[1,2] and Felix Felmy[1,2,3]

[1]Division of Neurobiology, [2]Graduate School of Systemic Neurosciences, and [3]Bioimaging Center, Department Biology II, Ludwig-Maximilians University Munich, D-82152 Martinsried, Germany

In the auditory system, large somatic synapses convey strong excitation that supports temporally precise information transfer. The information transfer of such synapses has predominantly been investigated in the endbulbs of Held in the anterior ventral cochlear nucleus and the calyx of Held in the medial nucleus of the trapezoid body. These large synapses either work as relays or integrate over a small number of inputs to excite the postsynaptic neuron beyond action potential (AP) threshold. In the monaural system, another large somatic synapse targets neurons in the ventral nucleus of the lateral lemniscus (VNLL). Here, we comparatively analyze the mechanisms of synaptic information transfer in endbulbs in the VNLL and the calyx of Held in juvenile Mongolian gerbils. We find that endbulbs in the VNLL are functionally surface-scaled versions of the calyx of Held with respect to vesicle availability, release efficacy, and synaptic peak currents. This functional scaling is achieved by different calcium current kinetics that compensate for the smaller AP in VNLL endbulbs. However, the average postsynaptic current in the VNLL fails to elicit APs in its target neurons, even though equal current suffices to generate APs in neurons postsynaptic to the calyx of Held. In the VNLL, a postsynaptic A-type outward current reduces excitability and prevents AP generation upon a single presynaptic input. Instead, coincidence detection of inputs from two converging endbulbs is ideal to reliably trigger APs. Thus, even large endbulbs do not guarantee one-to-one AP transfer. Instead, information flow appears regulated by circuit requirements.

Key words: **auditory system; endbulb synapse; postsynaptic integration; synaptic transmission; ventral nucleus of the lateral lemniscus**

Introduction

Large, somatic synapses in the auditory system convey information with high reliability and temporal precision (Trussell, 1999; von Gersdorff and Borst, 2002). At least three large mammalian auditory synapses are known. The endbulbs and modified endbulbs of Held terminate on bushy cells in the anterior ventral cochlear nucleus and arise from auditory nerve fibers (Liberman, 1991; Ryugo and Sento, 1991; Spirou et al., 2005). Calyces of Held in the medial nucleus of the trapezoid body (MNTB) are formed by axons from the globular bushy cells in the anterior ventral cochlear nucleus (Friauf and Ostwald, 1988; Smith et al., 1991). The endbulbs in the ventral nucleus of the lateral lemniscus (VNLL) appear to originate predominantly from axons emanating from the octopus cell area in the posterior ventral cochlear nucleus (Friauf and Ostwald, 1988; Vater and Feng, 1990; Adams, 1997; Schofield and Cant, 1997; Smith et al., 2005).

Anatomically and functionally large synapses in the VNLL are distinct from those in the anterior ventral cochlear nucleus and the MNTB, as they are suited to provide a rapid population-based onset inhibition to their target areas. This role is enabled by specific circuit properties. First, a conversion of an excitatory into an inhibitory signal takes place in the VNLL because these VNLL neurons are glycinergic (Saint Marie et al., 1997). Second, several endbulbs converge onto a single postsynaptic VNLL neuron (Covey and Casseday, 1986; Friauf and Ostwald, 1988; Vater and Feng, 1990; Adams, 1997; Schofield and Cant, 1997; Smith et al., 2005). Along the same line, neurons of the octopus cell area diverge on several VNLL neurons (Covey and Casseday, 1986; Vater and Feng, 1990; Adams, 1997; Schofield and Cant, 1997). Finally, neurons in the VNLL appear to inherit physiological properties from neurons in the octopus cell area as both are broadly tuned and preferentially spike to sound onsets (Godfrey et al., 1975; Rhode et al., 1983; Covey and Casseday, 1991; Smith et al., 2005; Zhang and Kelly, 2006).

A physiological hallmark in VNLL neurons, at least in bats, is the constant latency of onset spikes regardless of sound intensity and frequencies (Covey and Casseday, 1991). This feature has been suggested to arise through a synaptic coincidence detection mechanism (Covey and Casseday, 1991). Thus, it is unclear whether the endbulb synapses in the VNLL function more similarly to the relaying calyces and the large endbulbs of Held with a

Received Aug. 28, 2013; revised Jan. 16, 2014; accepted Jan. 22, 2014.

Author contributions: C.B., E.M.M.M., and F.F. designed research; C.B., E.M.M.M., and F.F. performed research; C.B., E.M.M.M., J.J.A., and F.F. analyzed data; C.B., E.M.M.M., J.J.A., and F.F. wrote the paper.

F.F. was supported by the Elisabeth and Helmut Uhl Foundation. J.J.A., C.B., and this work were supported by the Deutsche Forschungsgemeinschaft (FE789/3–1). We thank Prof. Benedikt Grothe for support and the introduction to the VNLL, Prof. Rainer Uhl for his support, and Prof. Hans Straka and Prof. Christian Leibold for comments on the manuscript.

The authors declare no competing financial interests.

*C.B. and E.M.M.M. contributed equally to this work.

Correspondence should be addressed to Dr. Felix Felmy, BioImaging Center, Department Biology I, Ludwig-Maximilians University Munich, Großhaderner Straße 2, D-82152 Martinsried, Germany. E-mail: felmy@zi.biologie.uni-muenchen.de.

DOI:10.1523/JNEUROSCI.3664-13.2014

 0270-6474/14/343237-10$15.00/0

one-to-one action potential (AP) transfer (Rothman et al., 1993; von Gersdorff and Borst, 2002; Yang and Xu-Friedman, 2010) or to the smaller endbulbs of Held that integrate multiple inputs to generate an AP (Rothman et al., 1993; Kuhlmann et al., 2002).

Here, we show that coincidence of paired inputs to juvenile VNLL neurons is ideal to generate reliable postsynaptic APs. Furthermore, by comparing the presynaptic size, firing behavior, release efficacy, synaptic transmission, and postsynaptic excitability of endbulbs in the VNLL with the calyx of Held, we conclude that, even at large synapses, information flow is controlled in a circuit-dependent manner.

Materials and Methods

Slice preparation. All experiments complied with institutional guidelines and national and regional laws. Slices were prepared from Mongolian gerbils (*Meriones unguiculatus*) of either sex from postnatal days 9–11 (see Figure 7 for postnatal day 14). After decapitation, brains were removed in dissection solution containing (in mM) as follows: 50 sucrose, 25 NaCl, 25 $NaHCO_3$, 2.5 KCl, 1.25 Na_2HPO_4, 3 $MgCl_2$, 0.1 $CaCl_2$, 25 glucose, 0.4 ascorbic acid, 3 myo-inositol, and 2 Na-pyruvate (pH 7.4 when bubbled with 95% O_2 and 5% CO_2). After trimming, transverse brainstem slices containing the VNLL or the MNTB were taken with a VT1200S vibratome (Leica). Slices were incubated in recording solution (same as dissection solution but with 125 mM NaCl, no sucrose, and 2 mM $CaCl_2$ and 1 mM $MgCl_2$) at 36°C for 45 min, bubbled with 5% CO_2 and 95% O_2).

Electrophysiology. After incubation, slices were transferred to a recording chamber attached to a microscope (BX50WI or BX51WI, Olympus) equipped with gradient contrast illumination and continuously perfused with recording solution. All recordings were performed at near physiological temperature (34°C–35°C). Presynaptic and postsynaptic compartments were visualized and imaged with a TILL Photonics system composed of an Imago or Retiga2000DC CCD camera, a monochromator, and its control unit. In single postsynaptic recordings, only VNLL and MNTB cells were selected that received a visually identified endbulb or calyx. Current-clamp and voltage-clamp whole-cell recordings were performed using an EPC10/2 amplifier (HEKA Elektronik). Presynaptic and postsynaptic access resistance was compensated to a residual of 3–4 MOhm and 2–2.5 MOhm, respectively. In current-clamp mode, the bridge balance was set to 100% after estimation of the access resistance. Data were acquired at 20–50 kHz and filtered at 3–4 kHz. Data were corrected offline for the calculated liquid junction potential (LJP) of each solution. The presynaptic current-clamp solution contained the following (in mM): 145 K-gluconate, 5 KCl, 15 K-HEPES, 3.3 $MgCl_2$, 2 K-ATP, 0.3 Na-GTP, 7 Na_2-phosphocreatine, adjusted to pH 7.2 with KOH, 16 mV LJP. The postsynaptic current-clamp solution contained the following (in mM): 145 K-gluconate, 5 KCl, 15 K-HEPES, 2 K-ATP, 2 Mg-ATP, 0.3 Na-GTP, 7.5 Na_2-phosphocreatine, 5 K-EGTA, adjusted to pH 7.2 with KOH, 16 mV LJP. The presynaptic voltage-clamp solution contained the following (in mM): 135 Cs-gluconate, 15 HEPES, 3.3 $MgCl_2$, 2 K-ATP, 0.3 Na-GTP, 7.5 Na_2-phosphocreatine, 20 tetraethylammonium chloride (TEA-Cl), and 40 μM Fura-4F adjusted to pH 7.2 with CsOH, 13 mV LJP. The postsynaptic voltage-clamp solution contained the following (in mM): 105 Cs-gluconate, 26.7 CsCl, 10 Cs-HEPES, 20 TEA-Cl, 3.3 $MgCl_2$, 2 Na_2-ATP, 0.3 Na-GTP, 3 Na_2-phosphocreatine, 5 Cs-EGTA, with 50–70 μM Alexa-568, adjusted to pH 7.2 with CsOH, 11 mV LJP. The internal solution for postsynaptic voltage-clamp recordings isolating potassium currents was the same as for postsynaptic current-clamp recordings. A-type potassium currents were pharmacologically and electrophysiologically isolated by applying a subtraction protocol. Step potentials of 500 ms length were preceded by either a −116 mV, 500 ms or a −36 mV, 500 ms conditioning potential. Inactivation of the transient potassium current was determined using a −36 mV test voltage command that was preceded by conditioning steps from −116 to −36 mV for 500 ms. In addition, the external solution contained Cd^{2+} (100 μM), ZD7288 (50 μM), TTX (0.5–1 μM), CPP (10 μM), DNQX (20 μM), strychnine (0.5 μM), and SR95531 (10 μM). To isolate presynaptic calcium currents and for presynaptic capacitance measurements, the recording solution contained TEA-Cl (10 mM), 4-aminopyridine (4-AP, 2 mM), ZD7288 (50 μM), TTX (0.5–1 μM), CPP (10 μM), DNQX (20 μM), strychnine (0.5 μM), and SR95531 (10 μM). Pharmacologically isolated presynaptic calcium currents were P/n corrected offline. Calcium current inactivation was assessed by a 300 ms holding command between −71 and −21 mV that was followed by a 200 ms test pulse of −11 mV holding potential. Capacitance recordings were performed according to Lindau and Neher (1988) implemented in the PatchMaster Software operating the lock-in amplifier of the EPC10/2, using a sine wave with 1 kHz frequency and 30 mV peak amplitude. For the calcium current capacitance increase, the terminals were clamped from −91 mV to 69 mV for 5 ms and held at −11 mV for the given stimulation time.

Image and data analysis. Single-terminal electroporation was performed as described previously for somata (Rautenberg et al., 2009). Image stacks of labeled terminals in postfixed tissue mounted in Vectashield were acquired with a Leica SP5 confocal system. Terminal surfaces were reconstructed from these image stacks in AMIRA 5.4.2 (Mercury Computer Systems; TGS Unit) using the brush and threshold tool from the segmentation editor. Electrophysiological recordings were analyzed in IGOR Pro (Wavemetrics) with custom-written macros. Results are presented as mean ± SEM. Significance was tested using a Student's *t* test as normal distributions were assumed.

Results

Presynaptic compartment size

The size of a presynaptic compartment is an important determinant for the number of active zones and hence for the maximal transmitter release. The size of the calyx of Held was compared with the endbulbs in the VNLL anatomically and electrophysiologically. Anatomical estimates were based on reconstructions of single electroporated nerve terminals (Fig. 1*A*,*B*). The reconstructed surface area of the calyx of Held is ~2-fold larger compared with the endbulbs in the VNLL (Fig. 1*C*; MNTB, $n = 9$; VNLL, $n = 7$). In agreement with previous evidence (Covey and Casseday, 1986; Vater and Feng, 1990; Adams, 1997; Schofield and Cant, 1997), two presynaptic terminals innervating one postsynaptic VNLL neuron were electroporated in four instances (Fig. 1*A*,*B*).

The size difference of the two terminals was further investigated by estimating the capacitance electrophysiologically in voltage clamp during blockage of sodium and potassium conductances to enhance membrane resistance (Fig. 1*D–F*). To determine the charging time of the terminal compartment, the fast decay time constant of the average current deflection was extracted from a biexponential fit (Fig. 1*D*). Endbulbs in the VNLL charged significantly faster compared with the calyces of Held (0.15 ± 0.01, $n = 29$ and 0.22 ± 0.02 ms, $n = 26$; $p < 0.01$; Fig. 1*E*). The compartment size of the calyx of Held, calculated from the charging transient and the enhanced membrane resistance according to Geiger and Jonas (2000), is ~1.7-fold larger than an endbulb in the VNLL (Fig. 1*F*; $p < 0.01$).

Finally, the passive properties of the presynaptic compartments of the calyx of Held ($n = 34$) and endbulb in the VNLL ($n = 28$) were compared by current-clamp recordings. The resting potentials of the calyx of Held and the VNLL endbulbs differ significantly ($p < 0.05$) with an average of −86.2 ± 0.9 mV and −80.5 ± 1.2 mV, respectively (Fig. 1*G*). The input resistance and membrane time constant (Fig. 1*G*,*H*) were significantly higher in the calyx of Held than in the endbulbs in the VNLL (297 ± 42 and 187 ± 17 MOhm, 9.0 ± 0.9 and 3.5 ± 0.3 ms, respectively, $p < 0.05$). From the membrane time constant and input resistance, the capacitance of these presynapses was calculated (Fig. 1*I*). This electronically effective capacitance was ~1.8-fold larger in calyx of Held synapses compared with endbulbs in the VNLL ($p < 0.05$).

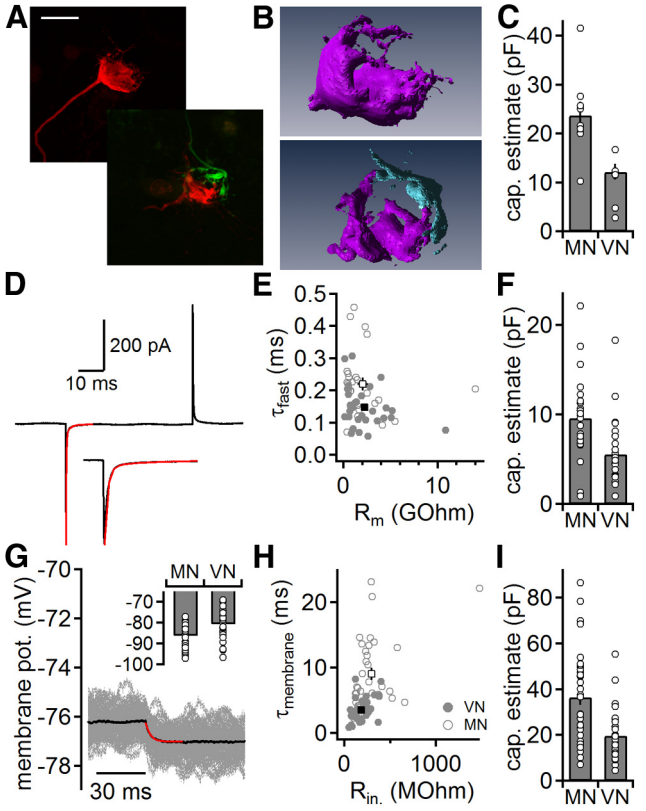

Figure 1. Size of somatic endbulbs in two auditory nuclei. ***A***, Calyx of Held (top) and two converging endbulbs in the VNLL (bottom). Images are maximal projections of confocal image stacks of individually electroporated endbulbs. Scale bar, 10 μm. ***B***, Reconstructions of the terminals shown in ***A***. Top, Calyx of Held. Bottom, Two endbulbs in the VNLL that converge onto the same postsynaptic neuron. ***C***, Endbulb capacitance estimated from reconstructions as shown in ***B***. ***D***, Presynaptic membrane current in response to a 10 mV hyperpolarization from −83 mV holding potential. Average trace (black) is derived from 150 repetitions. A biexponential fit (red) was used to extract the fast charging time constant. Inset, Magnification of the onset of the current response. ***E***, Fast time constant (τ_{fast}) as a function of the enhanced membrane resistance (R_m) in the calyx of Held (gray open symbols) and endbulbs in the VNLL (gray closed symbols); averages are given in black. ***F***, Endbulb capacitance estimated from voltage-clamp recordings as shown in ***D***. ***G***, Presynaptic membrane potential in response to a −5 pA current injection. Fifty single trials (gray) were averaged (black) and fitted with an exponential function (red) to extract the input resistance and the membrane time constant to estimate the capacitance. Inset, Presynaptic resting potential in the calyx of Held (MN) and endbulbs in the VNLL (VN). ***H***, Membrane time constant ($\tau_{membrane}$) as a function of the input resistance (R_{in}). Symbols as in ***E***. ***I***, Endbulb capacitance estimated from current-clamp recordings as shown in ***G***.

Together, the endbulbs in the VNLL are less hyperpolarized with lower resting input resistance and ~0.55-fold the size of the calyx of Held and show convergence onto a single VNLL neuron. In the following, the physiology of these different terminals was compared to investigate whether the anatomical differences are matched in function.

Presynaptic firing in the MNTB and VNLL

The properties of presynaptic APs influence the calcium influx and transmitter release. Therefore, fundamental AP properties and the input–output function were quantified to understand the presynaptic voltage signaling. In terminals in the MNTB (n = 35) and VNLL (n = 32), APs occurred only at the beginning of 500-ms-long depolarizations (Fig. 2*A*). Approximately 60% of all terminals responded with a single AP, whereas others generated up to three APs in accordance with multiple firing described previously (Forsythe, 1994). The subthreshold input–output functions showed outward rectification (Fig. 2B), clamping the

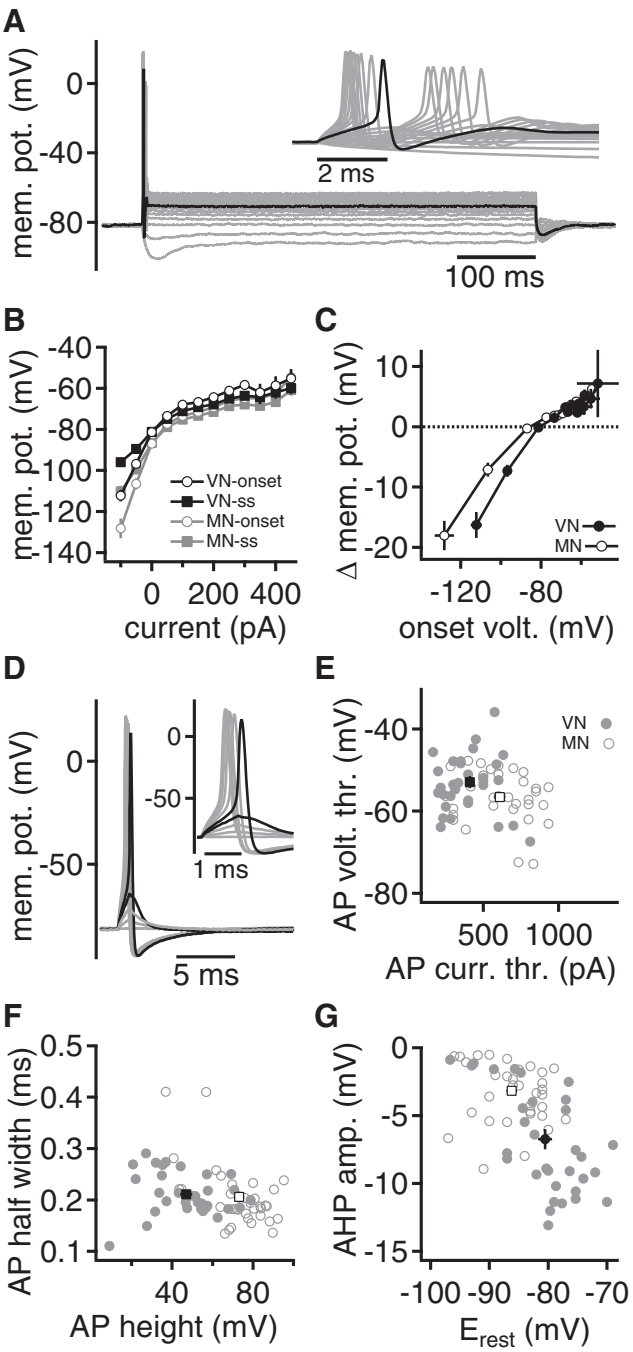

Figure 2. Presynaptic excitability of endbulbs in the VNLL and MNTB. ***A***, Voltage responses to 500 ms hyperpolarizing and depolarizing current injections in an endbulb in the VNLL. Inset, Onset of voltage response. First suprathreshold voltage response is given in black. Five of 17 endbulbs in the VNLL responded with an AP doublet during current injections. ***B***, Onset and steady-state voltage-current relationships in the endbulb in the VNLL (black) and the calyx of Held (gray). Onset voltage (open symbols) was calculated at the maximal hyperpolarization after the AP firing. Steady-state (ss) response was extracted at the end of the current injection. ***C***, Difference between onset and steady-state voltage response ($\Delta_{mem.\ pot.}$) as a function of the onset voltage. Closed symbols represent endbulbs in the VNLL, and open symbols represent calyx of Held recordings. ***D***, A brief, 1 ms current injection of increasing strength elicited subthreshold and suprathreshold responses in an endbulb in the VNLL. Last subthreshold and first suprathreshold responses are shown in black. Inset, Magnification of the time of AP generation. ***E***, The AP voltage threshold is given as a function of AP current threshold. Closed symbols represent single recordings from endbulbs in the VNLL, and open symbols represent calyx of Held recordings. Black square symbols represent the respective average values. ***F***, The AP half-width is given as a function of AP height. Symbols as in ***E***. ***G***, The AP after-hyperpolarization given as a function of membrane potential. Symbols as in ***E***.

steady-state voltage response to ~−56 mV. Consistent with the lower input resistance of endbulbs in the VNLL, the hyperpolarizing voltage deflection to equally large current injections was smaller compared with the calyces of Held (Fig. 2*B*). Both types of terminals responded with a voltage sag to hyperpolarizations (Fig. 2*A–C*). The voltage sags were analyzed as the difference between the hyperpolarization minimum to steady state (Fig. 2*C*). Significantly less hyperpolarization was required in VNLL terminals to generate a voltage sag compared with the calyx of Held (Fig. 2*C*; $p < 0.05$). This finding indicates that both terminals express a hyperpolarization-activated conductance, yet possibly with different kinetics and with a different degree of activation at their respective resting potentials.

To compare the AP properties in the calyx of Held with the endbulb in the VNLL, a 1 ms current pulse of increasing amplitude was injected (Fig. 2*D*) and the first suprathreshold response was analyzed (Couchman et al., 2010; Porres et al., 2011; Ammer et al., 2012). The average AP current threshold was larger and the voltage threshold lower in the calyx of Held (610 ± 36 pA; −40.6 ± 1.1 mV) compared with the endbulbs in the VNLL (410 ± 31 pA; −36.9 ± 1.4 mV; Fig. 2*E*; each $p < 0.05$). The AP height measured from voltage threshold, as well as from resting potential, was larger in the calyx of Held compared with the endbulbs in the VNLL (Fig. 2*F*; $p < 0.05$). However, no difference in AP half-width was observed (Fig. 2*F*). The after-hyperpolarization was smaller ($p < 0.05$) in the calyx of Held than in the endbulbs in the VNLL (Fig. 2*G*). As the after-hyperpolarization depends on potassium conductances, its size appeared to correlate with the resting potential (Fig. 2*G*). Thus, the variations in the size of the after-hyperpolarization might be explained by the different resting potentials of these terminals. Together, the excitability of the two terminals differs with respect to the AP voltage and current threshold, the latter being explained by the smaller terminal size and the lower input resistance (Ammer et al., 2012). Toward a comparison of the terminal function, the different AP heights are most crucial, as AP shape forms the basis of calcium channel opening, linking neuronal activity to transmitter release.

Calcium currents in synaptic terminals in the MNTB and VNLL

To understand how the calcium influx is coupled to the invading AP, the calcium currents in these nerve terminals were investigated (Fig. 3). The current–voltage relation was analyzed at the peak and at the steady-state current (Fig. 3*A–D*). The average peak calcium current in the calyx of Held ($n = 21$) was 2.2-fold larger compared with the endbulb of the VNLL ($n = 18$) (Fig. 3*C*,*D*). A similar twofold difference was present between the terminals' steady-state currents (Fig. 3*C*,*D*). This finding suggests, as the magnitude of the calcium current scales with terminal size, that it does not compensate for the difference in AP height.

Differences in the voltage-dependent activation could still compensate for the different AP heights. The time course of the voltage-dependent activation was measured as the time to peak of the calcium currents. The time to peak evoked by command potentials >−21 mV was equal for the calyx of Held and the endbulb in the VNLL (Fig. 3*E*). However, at more negative potentials, the endbulb in the VNLL activated faster compared with the calyx of Held. To gain more insight into the voltage-dependent opening, the inactivation kinetics were recorded. At half-activation a 4 mV leftward shift and at half-inactivation a 1.5 mV shift of the calcium currents in the endbulb of the VNLL ($n = 18$) compared with the calyx of Held ($n = 15$) exists (Fig. 3*F*). Thus, the voltage dependence of the calcium currents in these terminals might compensate for the difference in AP height to achieve a comparable calcium influx.

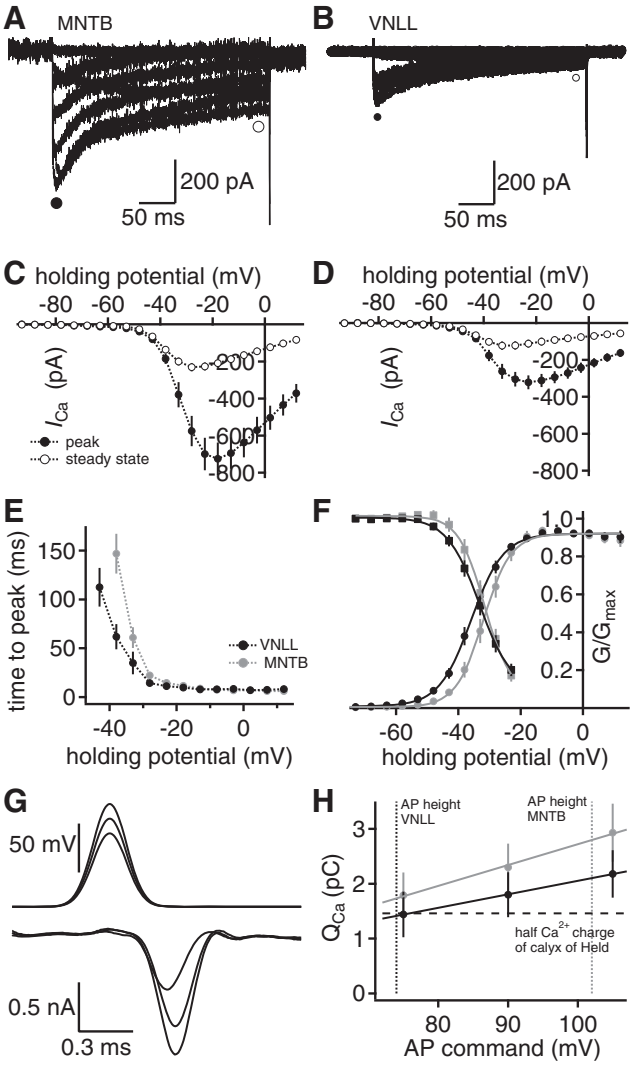

Figure 3. Activation and scaling of presynaptic calcium currents. ***A***, ***B***, Whole-cell calcium currents from a calyx of Held (***A***) and an endbulb in the VNLL (***B***). Closed circles represent the peak current, and open circles represent the regions at which the size of the steady-state currents was extracted. ***C***, ***D***, Current–voltage relationships in calyx of Held (***C***) and the endbulb in the VNLL (***D***). Closed symbols represent peak currents; open symbols represent steady-state values. ***E***, Voltage-dependent activation time of calcium currents (calyx of Held, $n = 21$; endbulbs in the VNLL, $n = 18$). ***F***, Voltage-dependent activation and inactivation of calcium currents in the calyx of Held (gray) and the endbulb in the VNLL (black). Lines indicate sigmoid fits. ***G***, Presynaptic calcium current (bottom) evoked by AP waveforms of different height (top) in an endbulb in the VNLL. ***H***, Average calcium current charge at different AP waveform commands in the endbulb in the VNLL (black symbols, $n = 6$) and the calyx of Held (gray solid symbols, $n = 8$). Dotted vertical lines indicate the average AP height in the endbulb in the VNLL (black) and the calyx of Held (gray). Horizontal dotted line indicates half of the calcium current charge of the calyx of Held.

To test the hypothesis that activation kinetics compensate for the smaller AP in the endbulbs in the VNLL, the calcium current charge evoked by mimicked AP voltage waveforms was determined (Fig. 3*G*,*H*). Waveforms mimicking the AP in the endbulb of the VNLL of 75 mV, the calyx of Held of 105 mV, and an intermediate AP height of 90 mV were applied as voltage commands (Fig. 3*G*,*H*). The charge of the calcium currents increased from the waveform of 75–105 mV from 1.79 ± 0.42 to 2.93 ± 0.53 pC in the calyx of Held ($n = 8$) and from 1.44 ± 0.42 to

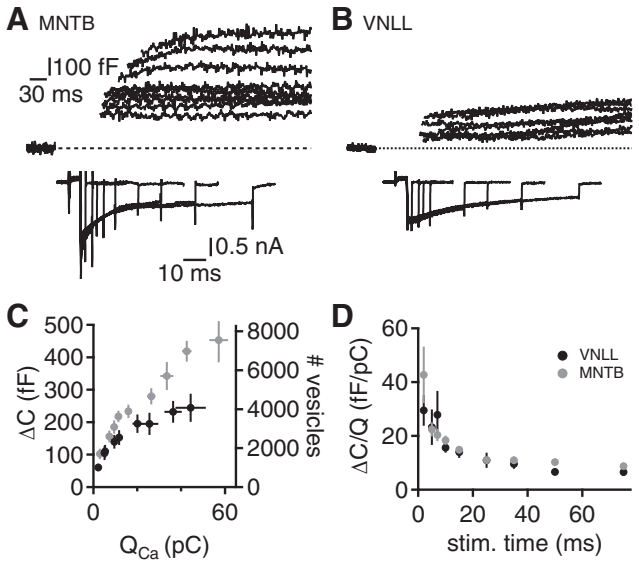

Figure 4. Release efficacy is size invariant. ***A***, ***B***, Presynaptic capacitance recordings from calyx of Held (***A***) and the endbulb in the VNLL (***B***). Top, Capacitance increase that was evoked by a presynaptic voltage step opening voltage-gated calcium currents (bottom). Same scale in ***A*** and ***B***. ***C***, Capacitance change (ΔC) and the estimated vesicle number are given as a function of the activated calcium charge (Q_{Ca}). Black symbols represent endbulbs in the VNLL ($n = 10–15$), and gray symbols represent calyx of Held ($n = 10$ 15) recordings. ***D***, The efficacy of release is given by the capacitance increase over the corresponding calcium charge evoked by the respective duration of depolarization. Symbols as in ***C***.

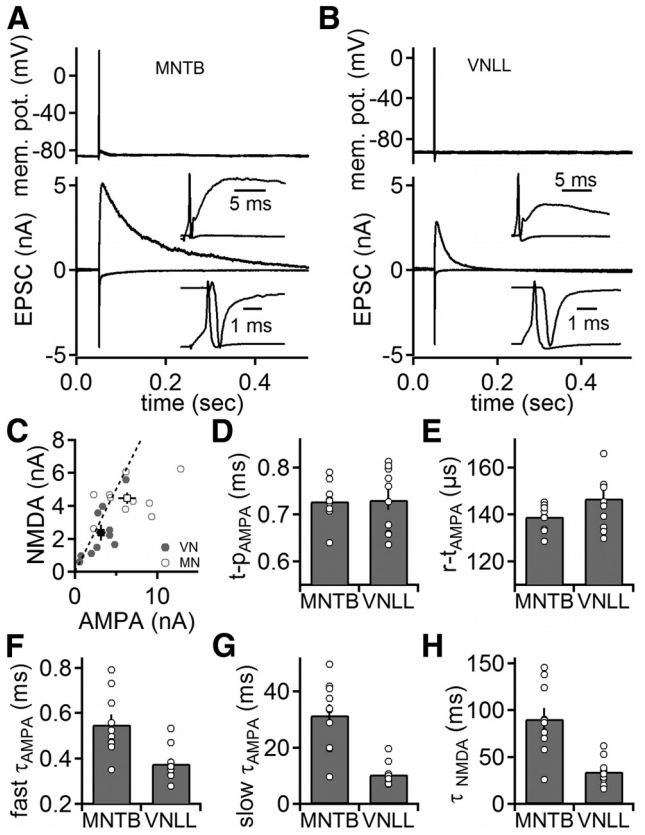

Figure 5. Synaptic currents in the VNLL and MNTB. ***A***, ***B***, Simultaneous presynaptic current-clamp (top) and postsynaptic voltage-clamp (bottom) recordings from calyx of Held (***A***) and endbulb synapses in the VNLL (***B***). Presynaptically evoked APs trigger fast EPSCs at a holding potential of −81 mV and slow EPSCs at 39 mV that are dominated by the AMPA and NMDA component, respectively. ***C***, Amplitude of the NMDA and AMPA response at the endbulb in the VNLL (closed symbols, $n = 10$) and the calyx of Held (open symbols, $n = 10$). Dashed line indicates unity. ***D***, Time to peak response (t-p) measured from the peak of the presynaptic AP to the peak of the postsynaptic AMPA response at the endbulbs in the VNLL and the calyx of Held. ***E***, Rise time (r-t) of the AMPA response at endbulbs in the VNLL and the calyx of Held. ***F***, ***G***, Fast (***F***) and slow (***G***) decay time constants of the AMPA response (τ_{AMPA}) at the endbulb in the VNLL and the calyx of Held. ***H***, Decay time constants of the NMDA response (τ_{NMDA}) at the endbulb in the VNLL and the calyx of Held.

2.18 ± 0.43 pC in the endbulbs in the VNLL ($n = 6$; Fig. 3*H*). The charge of the calcium current corresponding to half of the calyx of Held is activated in the endbulb in the VNLL at a 30 mV lower AP height (Fig. 3*H*). Thus, the AP evoked calcium influx scales with terminal size, most likely because of the differences in voltage-dependent activation of the calcium currents that compensate for the smaller AP in the endbulbs in the VNLL. This finding implies that the microdomain calcium signal that is driven by the calcium charge at a given surface area is similar for these two terminal types. Hence, vesicular release should scale again with the size of these terminals.

Vesicle availability

Synaptic transmission relies on the availability of synaptic vesicles and their release efficacy. The number of vesicles that can be released from the endbulb in the VNLL and the calyx of Held was assessed by the calcium-activated increases in terminal capacitance (Fig. 4*A*,*B*). The increase in capacitance as a function of the calcium current charge was always larger in the calyx of Held compared with the endbulb in the VNLL (Fig. 4*C*). The capacitance was converted into the number of vesicles by assuming a vesicle capacitance of 60 aF (Wu et al., 2007). The longest and the shortest depolarization step released 7547 ± 1142 and 1708 ± 262 vesicles in the calyx of Held and 4076 ± 726 and 1009 ± 187 vesicles in the endbulb in the VNLL, respectively. Thus, the calyx of Held released ~1.8-fold more vesicles compared with the endbulb in the VNLL. Next, the efficacy of vesicle release, defined as the ratio of fused vesicles over calcium charge for a given stimulation length, was compared (Fig. 4*D*). This analysis compensates for the different charge transfer at a given stimulation length and determines the relative vesicle release at a certain stimulation time. This release efficacy of both terminals was similar for all short depolarization lengths tested ($p > 0.05$, except at 50 ms stimulation length; Fig. 4*D*). Together, these data indicate that the calyx of Held and the endbulb in the VNLL are functionally surface-scaled versions of each other in respect to vesicle availability and release efficacy.

Synaptic transmission at large synapses in the MNTB and VNLL

To assay differences in synaptic transmission between the two terminals, dual recordings from presynaptic and postsynaptic compartments were performed. Synaptic transmission was induced by presynaptically elicited APs. Postsynaptic currents were recorded at holding potentials of −81 and 39 mV (Fig. 5*A*,*B*) referring to AMPA and NMDA currents, respectively. The peaks of evoked AMPA and NMDA currents were ~2-fold smaller in the VNLL (3.2 ± 0.6 and 2.4 ± 0.5 nA, respectively; $n = 10$) compared with the MNTB (6.4 ± 1.1 and 4.4 ± 0.4 nA, respectively; $n = 10$; $p < 0.05$; Fig. 5*C*), with a similar NMDA/AMPA ratio ($p > 0.05$).

The overall time course of synaptic transmission involves presynaptic and postsynaptic mechanisms. At the calyx of Held and the endbulbs in the VNLL, the time from the steepest slope of the AP repolarization to the EPSC peak (time to peak) was similar

(Fig. 5*D*; $p > 0.05$). This finding, together with the similarity of the rise times of AMPA currents (Fig. 5*E*; $p > 0.05$), indicates that the initial mechanisms of synaptic transmission are equivalent between the calyx of Held and endbulbs in the VNLL. At large somatic synapses, the EPSC decay time constants reflect predominantly postsynaptic mechanisms. The fast and slow decays of the AMPA component extracted from a biexponential fit were faster in the endbulb in the VNLL compared with the calyx of Held ($p < 0.05$; Fig. 5*F*, *G*). Furthermore, the fraction of the fast EPSC decay time constant was larger in the VNLL (0.88 ± 0.015) than in MNTB neurons (0.91 ± 0.01), leading to an overall slower weighted decay time constant in MNTB neurons (4.34 ± 0.69 ms and 1.23 ± 0.09 ms for MNTB and VNLL, respectively; $p < 0.05$). The time to peak of NMDA currents was significantly larger in MNTB (7.73 ± 0.54 ms) compared with VNLL neurons (5.08 ± 0.39 ms; $p < 0.05$). In addition, NMDA currents decayed ~2 times slower in MNTB principal cells (Fig. 5*H*). Overall, presynaptic mechanisms of synaptic transmission have a similar temporal profile in both types of terminals, whereas postsynaptic receptor activation is briefer in the VNLL than in the MNTB. This difference might be based on the different morphologies that allow glutamate to diffuse out of the synaptic cleft more rapidly in VNLL neurons (Fig. 1*A*,*B*) (Xu-Friedman and Regehr, 2004). This structure–function arrangement potentially leads to a temporally more precise excitatory drive in VNLL neurons. Furthermore, the size-scaled reduction in AMPA and NMDA charges of VNLL neurons transfers less excitatory drive to the postsynaptic partner.

Postsynaptic responsiveness

Next, we asked whether these two synapses provide a reliable one-to-one AP transfer in gerbils. Toward this aim, simultaneous current-clamp recordings from presynaptic and postsynaptic compartments were used to assay the reliability of AP transfer. In agreement with recordings in rats (Borst et al., 1995; Brew and Forsythe, 1995) and mice (Futai et al., 2001; Joshi and Wang, 2002), a single presynaptic AP reliably evoked a postsynaptic AP in each calyx of Held pair ($n = 6$; Fig. 6*A*). In contrast, only one of 16 pairs in the VNLL displayed a reliable one-to-one AP transfer. In 14 of 16 pairs, no AP was evoked; and in one pair only approximately every second trial relayed APs (Fig. 6*B*).

The mechanism underlying the failure of AP transfer in the VNLL was investigated using postsynaptic recordings. To probe for differences in the properties of the postsynaptic neurons in the MNTB and VNLL, a current waveform approximating a VNLL EPSC with a rise time of 0.18 ms and a decay time of 0.5 ms was injected. By injecting a waveform that approximates synaptic currents, a physiological current threshold can be estimated (Couchman et al., 2010; Ammer et al., 2012). The amplitude of this waveform was increased, and the first suprathreshold event was analyzed (Fig. 6*C*). The current threshold for MNTB neurons was low (1.89 ± 0.19 nA; Fig. 6*D*; $n = 8$), containing a threefold safety factor in regard to the recorded EPSC size (Fig. 5*C*). In contrast, the current threshold in VNLL neurons was high (3.48 ± 0.21 nA; Fig. 6*D*; $n = 7$). This current threshold is slightly larger than the average EPSCs (Fig. 5*C*), indicating no safety factor at all. Furthermore, the postsynaptic neurons in the VNLL had more negative resting potentials and higher voltage thresholds (Fig. 6*E*,*F*). Thus, the distance to the AP voltage threshold in VNLL neurons is 37.9 ± 2.3 mV compared with 28.6 ± 2.0 mV in MNTB neurons (Fig. 6*G*). In addition, the input resistance (228 ± 46 MOhm for MNTB and 254 ± 38 MOhm for VNLL neurons) and estimated capacitance (47 ± 8 pF for MNTB and 39 ± 4 pF for VNLL neurons) were similar in postsynaptic MNTB and VNLL neurons. Therefore, the difference in AP current threshold could arise either from a difference in the intrinsic excitability or from the differences in the membrane potential that has to be crossed.

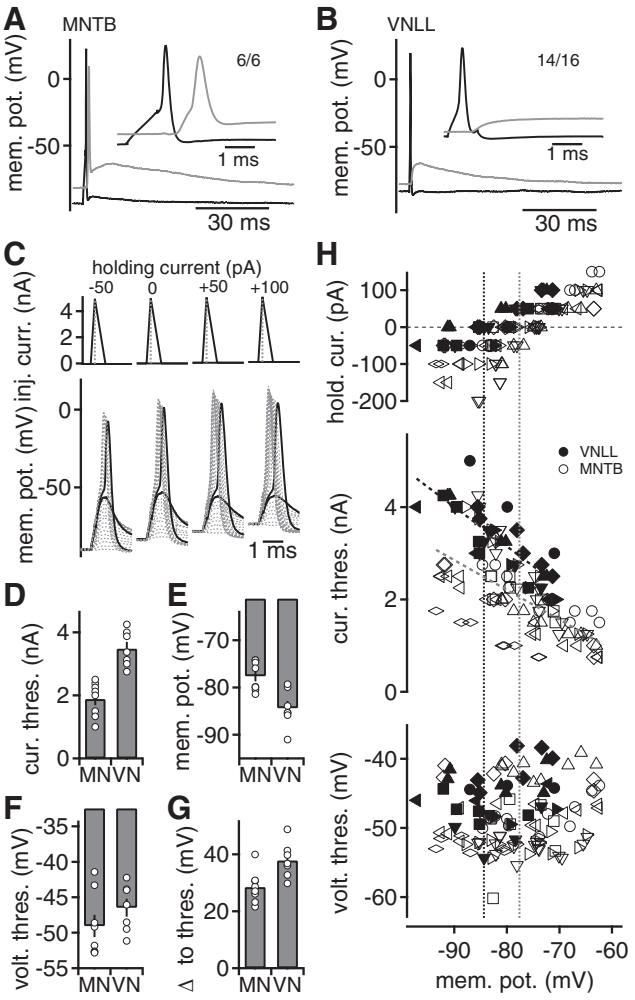

Figure 6. Postsynaptic excitability controls synaptic information transfer. ***A***, ***B***, Simultaneous presynaptic (black) and postsynaptic (gray) current-clamp recordings from calyx of Held (***A***) and endbulb synapses in the VNLL (***B***). Presynaptically evoked APs trigger postsynaptic voltage responses. Inset, presynaptic and postsynaptic response. ***A***, Numbers indicate cells that responded with a postsynaptic AP upon a presynaptic AP. ***B***, Numbers indicate the cells that showed no reliable AP transfer. ***C***, Postsynaptic current injections approximating EPSC waveforms were used to assay the current and voltage thresholds for APs at different offset holding currents. Top, Dotted lines indicate the successive increase in the peak current injection. Subthreshold and suprathreshold voltage responses of simulated EPSCs (bottom) in a VNLL neuron. ***D***, Postsynaptic current threshold of AP generation of simulated EPSC current injections in VNLL (VN) ($n = 7$) and MNTB (MN) ($n = 8$) neurons at 0 pA holding current. ***E***, Resting membrane potential of VNLL and MNTB neurons. ***F***, Postsynaptic voltage threshold of APs generated by injection of simulated EPSCs in the VNLL and the MNTB. ***G***, Difference between resting potential and voltage threshold for AP generation in VNLL and MNTB neurons at 0 pA holding current. ***H***, Current (middle) and voltage (bottom) threshold for the first suprathreshold response at different holding currents (top) as a function of the holding potential. Different symbols represent different cells. Closed symbols represent VNLL, and open symbols represent MNTB neurons. Dotted lines at the current threshold represent linear fits. Vertical dotted lines indicate the cell's average membrane potential.

To probe whether the excitability of the postsynaptic neurons underlies the different AP current thresholds, holding currents to alter the cells' resting potential were imposed upon the injection of EPSC waveforms (Fig. 6*C*). If the membrane potential is the

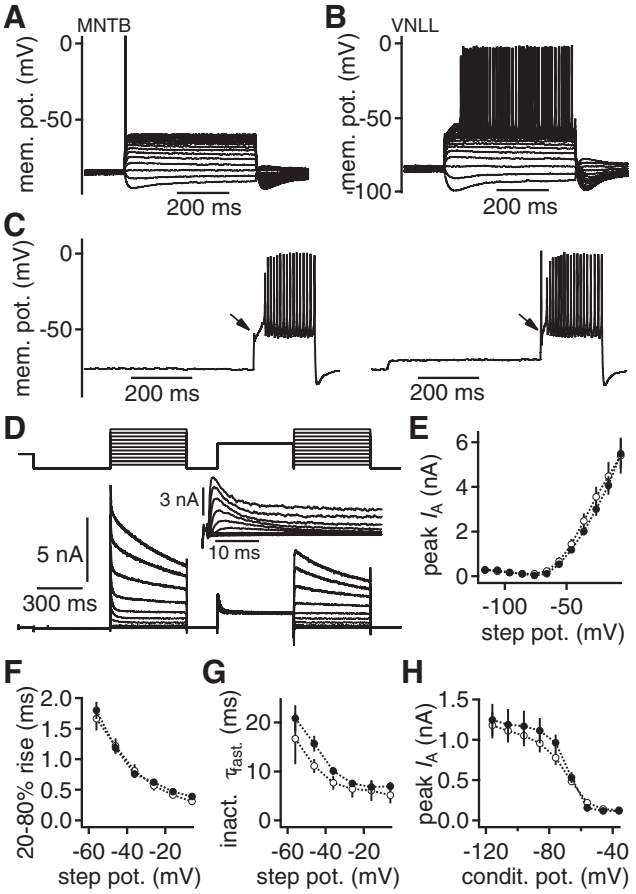

Figure 7. An inactivating postsynaptic potassium current gates information transfer. ***A***, ***B***, Postsynaptic voltage responses to 500 ms square current injections in neurons of the MNTB (***A***) and the VNLL (***B***). Hyperpolarizing responses appear similar. Suprathreshold injections induce different firing behaviors in MNTB and VNLL neurons. ***C***, The lack of onset APs (left) in VNLL neurons can be reversed by subthreshold depolarizations (right). ***D***, Postsynaptic voltage-clamp recording of a subtraction protocol used to isolate a transient potassium current (inset) in VNLL neurons. ***E***, Peak current of the isolated transient potassium current as a function of the step potential in VNLL neurons in P9–P11 (closed symbols, $n = 6$) and P14/P15 (open symbols, $n = 7$). ***F***, Rise time of the transient potassium current as a function of the step potential. Symbols as in ***E***. ***G***, Fast decay time constant (τ_{fast}) of the transient potassium current as a function of the step potential. Symbols as in ***E***. ***H***, Voltage-dependent inactivation of the transient potassium current as a function of the conditioning potential. Symbols as in ***E***.

main factor causing the different current thresholds, altering it should have a compensatory effect and hence lead to the same current threshold in MNTB and VNLL neurons. An overlapping range of membrane potentials was generated with holding currents of −200 to 100 pA (Fig. 6*H*). In both cell types, holding depolarizations reduced the AP current threshold. However, the current thresholds of VNLL and MNTB neurons remained segregated over the range tested, as indicated by linear fits (Fig. 6*H*). In addition, the voltage threshold was unaffected by the changes in membrane potential (Fig. 6*H*). Therefore, the difference in current threshold between the two cell types is based on excitability and might mediate the difference in reliability of the one-to-one AP transfer.

A potassium current controls postsynaptic excitability

To determine the excitability profiles of MNTB and VNLL neurons, input–output functions were recorded by step current injections. Depolarizing juvenile MNTB neurons led to a single AP at stimulation onset (Fig. 7*A*). The same current injections, however, induced continuous firing in juvenile VNLL neurons after a substantial delay that included a buildup of membrane depolarization (Fig. 7*B*). APs at stimulation onset without substantial delay could be elicited in VNLL neurons after a preceding subthreshold depolarization (Fig. 7*C*). As the onset of the response is most important for synaptic information transfer, we focused on the conductance that potentially explains this difference of the onset firing pattern. The slow buildup of membrane potential during the initial delay and the switch to an onset AP after preceding depolarization (Fig. 7*B*,*C*) indicated the presence of an inactivating, transient, fast A-type potassium current.

The presence of such an A-type current was tested electrophysiologically by recording pharmacologically isolated whole-cell potassium currents at different preceding holding potentials (Fig. 7*D*), thereby separating inactivating from noninactivating components. The current–voltage relation of the subtracted, inactivating potassium current (Fig. 7*D*, inset) showed that it activates at −66 mV and is 2.00 ± 0.17 nA at −36 mV (Fig. 7*E*; $n = 10$). This current rose rapidly and reached 20–80% rise times of 0.76 ± 0.06 ms at −36 mV (Fig. 7*F*). The fast component of the inactivation time constant was 10.08 ± 0.84 ms at −36 mV (Fig. 7*G*). In the same cells, the voltage-dependent inactivation was determined. The peak of the transient current was half-inactivated at −68 mV and showed nearly no sign of inactivation at the resting potential of these cells (Fig. 7*H*). Thus, this fast transient potassium current resembles an A-type current that is ideally suited to shunt AP generation. Hence, the postsynaptic A-type potassium current provides a gate for synaptic information transfer. As this current appears crucial for the excitability of VNLL neurons at P9-P11, its presence during the initial phase of late postnatal development was analyzed in P14/P15 animals. In this age group, the A-type current appeared nearly indistinguishable compared with P9-P11 only that it inactivated slightly faster (Fig. 7*E–H*).

Precise synaptic transmission is achieved by coincidence detection

A single AP of a single presynaptic fiber does not reliably drive a postsynaptic VNLL neuron. Thus, APs need to be triggered based on postsynaptic integration. There are two alternative integration modes that could lead to postsynaptic AP generation. First, inactivating the A-type current by temporal integration of a repetitively activated single input could finally result in a postsynaptic AP. Second, the morphological arrangement of two or more converging endbulbs could be used for coincidence detection if presynaptic activity is temporally matched. The preferred integration mode was tested with simultaneous presynaptic and postsynaptic current-clamp recordings.

To test for temporal integration of a single input, five presynaptic APs were elicited with suprathreshold current injections at 100 or 200 Hz (Fig. 8*A*). The postsynaptic voltage response summed during the train and occasionally elicited postsynaptic APs. For 100 Hz trains, only 3 of 10 and for 200 Hz 4 of 10 recordings elicited a postsynaptic AP (Fig. 8*B*). These postsynaptic APs occurred at various pulse numbers during the stimulation train (Fig. 8*B*) and were thus temporally imprecise. Together, the temporal integration mode as shown here appears not to match the constant onset latency *in vivo* (Covey and Casseday, 1991) and is not suited for a fast, temporally precise feedforward inhibition provided by the VNLL (Nayagam et al., 2005; Xie et al., 2007).

Doubling the size of the AMPA current with two coincidental inputs, in agreement with morphological results (Fig. 1*A*,*B*),

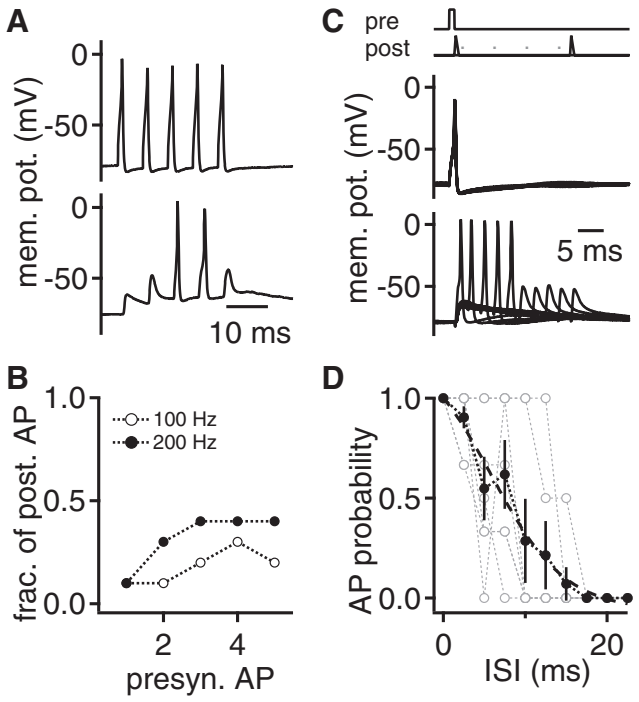

Figure 8. Efficacy of postsynaptic coincidence detection. ***A***, Temporal summation: Presynaptic (black) and postsynaptic (gray) current-clamp recording from an endbulb synapse in the VNLL. Five consecutive presynaptic APs were evoked by 1 ms current injections. ***B***, The fraction of postsynaptic neurons that generate an AP upon presynaptic stimulation as a function of stimulus number. Closed symbols represent 200 Hz stimulation ($n = 10$), and open symbols represent 100 Hz stimulation ($n = 10$). ***C***, Coincidence detection: A presynaptic evoked AP was paired with a subthreshold postsynaptic EPSC-like current injection. See stimulation protocol on top. Time interval between both stimuli was varied between 0 and 22.5 ms to determine the time window of suprathreshold summation. ***D***, AP probability as a function of the interstimulus time interval (ISI) from (***C***). Open gray symbols represent single cells; black symbols represent average over $n = 9$ cells. Dashed line indicates a sigmoid fit to the average data.

would be expected to result in suprathreshold excitation (Figs. 5 and 7). Thus, this synapse might act as a coincidence detector. This coincidence detection was tested by pairing a presynaptic AP with a postsynaptic current injection approximating a subthreshold AMPA-mediated EPSC (Fig. 8*C*). In addition, the time interval between these stimuli was varied. For short time intervals, the combination of the two stimuli reliably elicited a postsynaptic AP (Fig. 8*C*,*D*). The 50% AP probability was reached at an interstimulus interval of 7.5 ms (Fig. 8*D*). Together, these data show that the endbulbs in the VNLL appear to act as synaptic coincidence detector rather than simple relays. This coincidence detection is in line with the postulated synaptic integration mechanism derived from *in vivo* recordings in bats (Covey and Casseday, 1991) and meets the requirements of fast, temporally precise feedforward inhibition (Nayagam et al., 2005; Xie et al., 2007).

Discussion

We showed that endbulbs in the VNLL use a coincidence detection mechanism to generate temporally precise action potentials. Our experiments demonstrate that the EPSC generated by a single endbulb is insufficient to depolarize the postsynaptic neuron above AP threshold. The postsynaptic excitability in these juvenile VNLL neurons is partially determined by an A-type potassium current preventing a one-to-one AP transfer at stimulation onset. Interestingly, the amount of synaptic current generated by a single VNLL endbulb is sufficient to depolarize MNTB neurons beyond firing threshold. Hence, the mode of AP transfer in the VNLL is determined by the circuit requirement and terminal size is less crucial.

Maintained presynaptic structure–function relationship

The endbulb of the VNLL is ~0.55-fold the size of the calyx of Held. This estimation, together with recent data from mice (Lin et al., 2011), allows the rough comparison of three large synapses in the auditory brainstem at postnatal day 10. It appears that the smallest synapse is the endbulb of Held followed by the endbulb in the VNLL and then by the calyx of Held.

Endbulbs in the VNLL differ from calyces of Held not only in the effective surface area and lower input resistance that allows the terminals to charge faster, but also in the smaller AP height. A speculation consistent with our data is that the last hemi-node at which the AP is finally regenerated (Leão et al., 2005) is further distal to the terminals in the VNLL than in the calyx of Held. Thus, by this larger distance, the invading APs may be more attenuated in endbulbs in the VNLL.

The presynaptic AP height and shape are important for synaptic transmission, as they are directly linked with transmitter release through the gating of presynaptic voltage-gated calcium channels and the subsequent calcium influx. The smaller AP height in the endbulbs in the VNLL suggests lower release rates compared with the calyx of Held, as less calcium channels open and hence less calcium influx is predicted. However, the release efficacy and the EPSC size scale with the size of these terminals. This apparent contradiction is resolved by taking the kinetics of the voltage-gated calcium currents into account. The voltage-dependent activation and inactivation of the calcium current are shifted to more negative potentials, and the activation time is faster in the endbulb in the VNLL compared with the calyx of Held. These differences can compensate for the smaller AP and allow for the observed scaling of calcium charge transfer. Thus, the average microdomain calcium signal might be similar in the different terminals.

From the comparison of the structure–function relationship of presynaptic terminals, it can be inferred that the average active zones in different large synapses follow an anatomical blueprint. This blueprint is in line with the whole-cell scaling of the calcium current amplitude, the vesicle availability, the similarity in release efficacy, and the synaptic delay. Thus, despite possible intraterminal active zone variations (Sheng et al., 2012), our data from large auditory synapses support an ordered arrangement of presynaptic active zones that harbor a specified number of calcium channels (Cao et al., 2004; Zhai and Bellen, 2004) with distinct kinetics.

Postsynaptic gate for information transfer at large synapses

At large somatic, auditory synapses, the postsynaptic AP is driven by a synaptic conductance based on the release of a large number of vesicles from a single presynaptic terminal. The synaptic current generated by the calyx of Held contains a threefold safety factor to drive an AP in juvenile MNTB neurons. However, in juvenile VNLL neurons, no safety factor for AP transfer exists. Therefore, juvenile postsynaptic VNLL neurons do not reliably generate an AP upon a single presynaptic AP or a current injection approximating the average EPSC waveform. A one-to-one AP transfer is prevented by the low postsynaptic excitability based on elevated AP current and voltage thresholds, mediated partially by a transient potassium A-type current. The voltage-dependent activation and inactivation as well as the temporal kinetics of this current are ideally suited to counteract the onset of the synaptically induced depolarization. This postsynaptic gate

can be opened by a predepolarization leading to the inactivation of the A-type current. This mechanism leaves ample room for modulatory actions that lead to prolonged depolarizations of auditory brainstem neurons, such as the activation of metabotropic glutamate (Ene et al., 2003; Chanda and Xu-Friedman, 2011) or purinergic receptors (Milenkovic et al., 2009). Ongoing excitatory input from cells in the octopus cell area, which can fire at high rates (Godfrey et al., 1975; Rhode et al., 1983; Smith et al., 2005), could similarly lead to the inactivation of this A-type current, opening the gate for information transfer. This scenario is consistent with our results but leads only to a temporally imprecise activation of VNLL neurons.

The effectiveness of the postsynaptic gate can be illustrated by segregating temporal and spatial integration profiles in VNLL neurons. VNLL neurons are preferentially activated suprathreshold by the summation of two large inputs arriving with short time disparities rather than by the repetitive activation of a single presynaptic endbulb. Furthermore, the paired activation conserves the timing of the inputs better compared with the repetitive activation of a single input that leads to postsynaptic firing by inactivation of A-type currents. Thus, juvenile VNLL neurons that receive endbulbs appear ideal coincidence detectors rather than integrators of sustained activity or simple synaptic relays.

Compared with the coincidence detector neurons in the medial superior olive, which receive dendritic excitation and somatic inhibition (Clark, 1969; Couchman et al., 2012), VNLL neurons in gerbils receive their main excitatory inputs on the soma. This morphological difference might reflect the difference in integrational properties and detection tasks of these neurons. Neurons in the medial superior olive integrate their inputs to extract and compare temporal disparities of the incoming signals in the microsecond range, whereas VNLL neurons might serve to detect whether sufficient auditory broadband input is present to prime neurons in the inferior colliculus. This difference in postsynaptic integration is consistent with the differences in passive and active subthreshold membrane properties of neurons in the medial superior olive (Scott et al., 2005; Chirila et al., 2007; Couchman et al., 2010) and in the VNLL. Neurons in the medial superior olive integrate at least 2–4 fast excitatory inputs with extremely fast membrane time constants (Couchman et al., 2010) with large, balanced conductances of a low-voltage-activated potassium and a hyperpolarization activated cation current (Golding and Oertel, 2012). VNLL neurons appear much more passive at rest with little conductance of such channels. Furthermore, the comparison of interaural time disparities in medial superior olive neurons might be facilitated by the anatomical segregation of the excitatory inputs (Agmon-Snir et al., 1998) and their separation by inhibition (Grothe, 2003). Thus, the morphological arrangement of coincidence detector neurons might be adjusted to the specific detection task.

Implications for circuit function

At the developmentally immature stage at which our recordings were performed, the endbulbs in the VNLL are ideally suited to detect incoming activity of at least two large synapses within a short time window. This form of coincidence detection is in agreement with the constant onset latency and the synaptic arrangements found in mature bats (Covey and Casseday, 1986, 1991). We therefore speculate that this functional synaptic arrangement is maintained during circuit maturation in gerbils. If maintained, the function and morphological arrangement of the inputs from the octopus cell area (Godfrey et al., 1975; Rhode et al., 1983; Friauf and Ostwald, 1988; Vater and Feng, 1990; Adams, 1997; Schofield and Cant, 1997; Smith et al., 2005) and the functionality of this endbulb synapse reported here are ideal to generate a fast, broadband population signal in the VNLL. This population signal is transferred into the inferior colliculus as broadly tuned inhibition. Therefore, this inhibition is likely imposed on a population of neurons across different frequency regions in the inferior colliculus. Consistent with this circuit view, inhibition preceding the onset of excitation has been observed in the inferior colliculus (Nayagam et al., 2005; Xie et al., 2007). Therefore, the inhibition generated by VNLL neurons is ideally suited to produce a general reset signal in the inferior colliculus that might modulate the gain and the temporal profile of summed PSPs of early excitation. Thus, the postsynaptic gate of information transfer at the endbulb synapse in the VNLL might support secure, fast information processing in the inferior colliculus.

References

Adams JC (1997) Projections from octopus cells of the posteroventral cochlear nucleus to the ventral nucleus of the lateral lemniscus in cat and human. Auditory Neurosci 3:335–350.

Agmon-Snir H, Carr CE, Rinzel J (1998) The role of dendrites in auditory coincidence detection. Nature 393:268–272. CrossRef Medline

Ammer JJ, Grothe B, Felmy F (2012) Late postnatal development of intrinsic and synaptic properties promotes fast and precise signaling in the dorsal nucleus of the lateral lemniscus. J Neurophysiol 107:1172–1185. CrossRef Medline

Borst JG, Helmchen F, Sakmann B (1995) Pre- and postsynaptic whole-cell recordings in the medial nucleus of the trapezoid body of the rat. J Physiol 489:825–840. Medline

Brew HM, Forsythe ID (1995) Two voltage-dependent K+ conductances with complementary functions in postsynaptic integration at a central auditory synapse. J Neurosci 15:8011–8022. Medline

Cao YQ, Piedras-Rentería ES, Smith GB, Chen G, Harata NC, Tsien RW (2004) Presynaptic Ca^{2+} channels compete for channel type-preferring slots in altered neurotransmission arising from Ca^{2+} channelopathy. Neuron 43:387–400. CrossRef Medline

Chanda S, Xu-Friedman MA (2011) Excitatory modulation in the cochlear nucleus through group I metabotropic glutamate receptor activation. J Neurosci 31:7450–7455. CrossRef Medline

Chirila FV, Rowland KC, Thompson JM, Spirou GA (2007) Development of gerbil medial superior olive: integration of temporally delayed excitation and inhibition at physiological temperature. J Physiol 584:167–190. CrossRef Medline

Clark GM (1969) The ultrastructure of nerve endings in the medial superior olive of the cat. Brain Res 14:293–305. CrossRef Medline

Couchman K, Grothe B, Felmy F (2010) Medial superior olivary neurons receive surprisingly few excitatory and inhibitory inputs with balanced strength and short-term dynamics. J Neurosci 30:17111–17121. CrossRef Medline

Couchman K, Grothe B, Felmy F (2012) Functional localization of neurotransmitter receptors and synaptic inputs to mature neurons of the medial superior olive. J Neurophysiol 107:1186–1198. CrossRef Medline

Covey E, Casseday JH (1986) Connectional basis for frequency representation in the nuclei of the lateral lemniscus of the bat Eptesicus fuscus. J Neurosci 6:2926–2940. Medline

Covey E, Casseday JH (1991) The monaural nuclei of the lateral lemniscus in an echolocating bat: parallel pathways for analyzing temporal features of sound. J Neurosci 11:3456–3470. Medline

Ene FA, Kullmann PH, Gillespie DC, Kandler K (2003) Glutamatergic calcium responses in the developing lateral superior olive: receptor types and their specific activation by synaptic activity patterns. J Neurophysiol 90:2581–2591. CrossRef Medline

Forsythe ID (1994) Direct patch recording from identified presynaptic terminals mediating glutamatergic EPSCs in the rat CNS, in vitro. J Physiol 479:381–387. Medline

Friauf E, Ostwald J (1988) Divergent projections of physiologically characterized rat ventral cochlear nucleus neurons as shown by intra-axonal injection of horseradish peroxidase. Exp Brain Res 73:263–284. Medline

Futai K, Okada M, Matsuyama K, Takahashi T (2001) High-fidelity trans-

mission acquired via a developmental decrease in NMDA receptor expression at an auditory synapse. J Neurosci 21:3342–3349. Medline

Geiger JR, Jonas P (2000) Dynamic control of presynaptic Ca(2+) inflow by fast-inactivating K(+) channels in hippocampal mossy fiber boutons. Neuron 28:927–939. CrossRef Medline

Godfrey DA, Kiang NY, Norris BE (1975) Single unit activity in the posteroventral cochlear nucleus of the cat. J Comp Neurol 162:247–268. CrossRef Medline

Golding NL, Oertel D (2012) Synaptic integration in dendrites: exceptional need for speed. J Physiol 590:5563–5569. CrossRef Medline

Grothe B (2003) New roles for synaptic inhibition in sound localization. Nat Rev Neurosci 4:540–550. CrossRef Medline

Joshi I, Wang LY (2002) Developmental profiles of glutamate receptors and synaptic transmission at a single synapse in the mouse auditory brainstem. J Physiol 540:861–873. CrossRef Medline

Kuhlmann L, Burkitt AN, Paolini A, Clark GM (2002) Summation of spatiotemporal input patterns in leaky integrate-and-fire neurons: application to neurons in the cochlear nucleus receiving converging auditory nerve fiber input. J Comput Neurosci 12:55–73. CrossRef Medline

Leão RM, Kushmerick C, Pinaud R, Renden R, Li GL, Taschenberger H, Spirou G, Levinson SR, von Gersdorff H (2005) Presynaptic Na^+ channels: locus, development, and recovery from inactivation at a high-fidelity synapse. J Neurosci 25:3724–3738. CrossRef Medline

Liberman MC (1991) Central projections of auditory-nerve fibers of differing spontaneous rate: I. Anteroventral cochlear nucleus. J Comp Neurol 313:240–258. CrossRef Medline

Lin KH, Oleskevich S, Taschenberger H (2011) Presynaptic Ca^{2+} influx and vesicle exocytosis at the mouse endbulb of Held: a comparison of two auditory nerve terminals. J Physiol 589:4301–4320. Medline

Lindau M, Neher E (1988) Patch-clamp techniques for time-resolved capacitance measurements in single cells. Pflugers Arch 411:137–146. CrossRef Medline

Milenkovic I, Rinke I, Witte M, Dietz B, Rübsamen R (2009) P2 receptor-mediated signaling in spherical bushy cells of the mammalian cochlear nucleus. J Neurophysiol 102:1821–1833. CrossRef Medline

Nayagam DA, Clarey JC, Paolini AG (2005) Powerful, onset inhibition in the ventral nucleus of the lateral lemniscus. J Neurophysiol 94:1651–1654. CrossRef Medline

Porres CP, Meyer EM, Grothe B, Felmy F (2011) NMDA currents modulate the synaptic input–output functions of neurons in the dorsal nucleus of the lateral lemniscus in Mongolian gerbils. J Neurosci 31:4511–4523. CrossRef Medline

Rautenberg PL, Grothe B, Felmy F (2009) Quantification of the three-dimensional morphology of coincidence detector neurons in the medial superior olive of gerbils during late postnatal development. J Comp Neurol 517:385–396. CrossRef Medline

Rhode WS, Oertel D, Smith PH (1983) Physiological response properties of cells labeled intracellularly with horseradish peroxidase in cat ventral cochlear nucleus. J Comp Neurol 213:448–463. CrossRef Medline

Rothman JS, Young ED, Manis PB (1993) Convergence of auditory nerve fibers onto bushy cells in the ventral cochlear nucleus: implications of a computational model. J Neurophysiol 70:2562–2583. Medline

Ryugo DK, Sento S (1991) Synaptic connections of the auditory nerve in cats: relationship between endbulbs of Held and spherical bushy cells. J Comp Neurol 305:35–48. CrossRef Medline

Saint Marie RL, Shneiderman A, Stanforth DA (1997) Patterns of gamma-aminobutyric acid and glycine immunoreactivities reflect structural and functional differences of the cat lateral lemniscal nuclei. J Comp Neurol 389:264–276. CrossRef Medline

Schofield BR, Cant NB (1997) Ventral nucleus of the lateral lemniscus in guinea pigs: cytoarchitecture and inputs from the cochlear nucleus. J Comp Neurol 379:363–385. CrossRef Medline

Scott LL, Mathews PJ, Golding NL (2005) Posthearing developmental refinement of temporal processing in principal neurons of the medial superior olive. J Neurosci 25:7887–7895. CrossRef Medline

Sheng J, He L, Zheng H, Xue L, Luo F, Shin W, Sun T, Kuner T, Yue DT, Wu LG (2012) Calcium-channel number critically influences synaptic strength and plasticity at the active zone. Nat Neurosci 15:998–1006. CrossRef Medline

Smith PH, Joris PX, Carney LH, Yin TC (1991) Projections of physiologically characterized globular bushy cell axons from the cochlear nucleus of the cat. J Comp Neurol 304:387–407. CrossRef Medline

Smith PH, Massie A, Joris PX (2005) Acoustic stria: anatomy of physiologically characterized cells and their axonal projection patterns. J Comp Neurol 482:349–371. CrossRef Medline

Spirou GA, Rager J, Manis PB (2005) Convergence of auditory-nerve fiber projections onto globular bushy cells. Neuroscience 136:843–863. CrossRef Medline

Trussell LO (1999) Synaptic mechanisms for coding timing in auditory neurons. Annu Rev Physiol 61:477–496. CrossRef Medline

Vater M, Feng AS (1990) Functional organization of ascending and descending connections of the cochlear nucleus of horseshoe bats. J Comp Neurol 292:373–395. CrossRef Medline

von Gersdorff H, Borst JG (2002) Short-term plasticity at the calyx of Held. Nat Rev Neurosci 3:53–64. CrossRef Medline

Wu XS, Xue L, Mohan R, Paradiso K, Gillis KD, Wu LG (2007) The origin of quantal size variation: vesicular glutamate concentration plays a significant role. J Neurosci 27:3046–3056. CrossRef Medline

Xie R, Gittelman JX, Pollak GD (2007) Rethinking tuning: in vivo whole-cell recordings of the inferior colliculus in awake bats. J Neurosci 27:9469–9481. CrossRef Medline

Xu-Friedman MA, Regehr WG (2004) Structural contributions to short-term synaptic plasticity. Physiol Rev 84:69–85. CrossRef Medline

Yang H, Xu-Friedman MA (2010) Developmental mechanisms for suppressing the effects of delayed release at the endbulb of Held. J Neurosci 30:11466–11475. CrossRef Medline

Zhai RG, Bellen HJ (2004) The architecture of the active zone in the presynaptic nerve terminal. Physiology 19:262–270. CrossRef Medline

Zhang H, Kelly JB (2006) Responses of neurons in the rat's ventral nucleus of the lateral lemniscus to monaural and binaural tone bursts. J Neurophysiol 95:2501–2512. CrossRef Medline